Histone deacetylase 3-mediated histone deacetylation combined with activating transcription factor 3 promotes renal fibrosis by inhibiting Klotho

ZHIYING YANG[1,2], XUELING WANG[3,4], WENHONG LI[1], HAO CHEN[1] and GANG LIU[3,4]

[1]Department of Nephrology, Yan'an Hospital Affiliated to Kunming Medical University, Kunming, Yunnan 650051, P.R. China; [2]Key Laboratory of Tumor Immunological Prevention and Treatment of Yunnan Province, Yan'an Hospital Affiliated to Kunming Medical University, Kunming, Yunnan 650051, P.R. China; [3]Department of Nephrology, The Second Qilu Hospital of Shandong University, Jinan, Shandong 250033, P.R. China; [4]Nephrology Research Institute of Shandong University, Jinan, Shandong 250033, P.R. China

Received October 27, 2025; Accepted June 30, 2026

DOI: 10.3892/mmr.2026.13985

Abstract. Renal fibrosis is a representative pathological trait of renal aging and chronic kidney disease. However, the regulatory mechanisms of histone deacetylation in renal fibrosis remain unclear. A mouse renal fibrosis model was constructed using the unilateral ureteric obstruction method, and HK2 cells treated with TGF-β were used to create a renal fibrosis cell model. Low expression of Klotho in renal fibrosis is associated with histone deacetylase 3 (HDAC3)-mediated histone deacetylation. After TGF-β treatment, H3K9ac and Klotho binding was markedly decreased, while H3K9ac was enriched in the Klotho group after the addition of the HDAC3 inhibitor. Further experiments demonstrated that HDAC3 binding activates transcription factor 3, inhibits Klotho transcription and promotes cellular renal fibrosis. The absence of Klotho may activate the Wnt/β-catenin and NF-κB pathways to promote oxidative stress and inflammation, thereby exacerbating the fibrotic process. HDAC3 binds to ATF3 to transcriptionally repress Klotho, leading to activation of the Wnt/β-catenin and NF-κB pathways and exacerbation of renal fibrosis.

Introduction

Chronic kidney disease (CKD) is a growing public health problem due to its high prevalence and mortality. Globally, the number of adults with CKD was 788 million in 2023, with an age-standardised prevalence of 14.2%. CKD is currently the ninth leading cause of death worldwide, accounting for 1.48 million deaths annually (1). Renal fibrosis is a representative pathological trait of renal aging and CKD and is characterized by myofibroblast transdifferentiation (MTD) and excessive deposition of extracellular matrix (ECM) proteins in the renal interstitium (2). Kidney fibrosis is regulated by the interaction between profibrotic and antifibrotic signals and regulatory factors. Profibrotic pathways such as the TGFβ/Smad and Wnt/β-catenin pathways facilitate MTD and ECM (3), while fibrosis inhibitors such as Klotho, BMP-7 or Smad6/7 can clog or disturb profibrotic pathways. Moreover, patients with CKD with the same basic disease have different susceptibilities and severities of renal fibrosis (4). To date, the underlying mechanisms of renal fibrosis remain unclear. Therefore, probing the molecular mechanisms of renal fibrosis is key.

The Klotho protein family comprises three isoforms (α, β and γ). The present study focuses on αKlotho, which is predominantly expressed in the kidney and has well-established anti-fibrotic and anti-aging properties in the renal tubular epithelium. In the context of renal fibrosis and CKD research, the term 'Klotho' without a prefix has been widely accepted to refer specifically to αKlotho. Therefore, the present study and all subsequent references to 'Klotho' refer to αKlotho. Klotho-deficient mice exhibit multifarious aging phenotypes in the majority of organs and naturally develop kidney fibrosis (5). Klotho is a pivotal negative modulator of the Wnt pathway. It restrains kidney fibrosis by binding to the Wnt receptor, thereby inhibiting the profibrotic Wnt/β-catenin pathway (6). Second, some studies have shown that aging-associated inflammation and the progression of early CKD may be interrelated with the downregulation of Klotho and the induction of the RIG-I/NF-κB pathway (7). In diabetic db/db mice, Klotho expression was decreased in the kidney and corresponded to increased NF-κB activation (8). The mechanism of action and downstream targets of Klotho in renal fibrosis have been extensively explored. However, the upstream regulatory mechanisms of Klotho have rarely been reported.

The majority of studies have shown that histone modifications may also mediate pathways involved in CKD and fibrosis. Sun *et al* (9) reported that TGF-β increased histone H3 lysine methylation (H3K4me1, H3K4me2 and H3K4me3) and

Correspondence to: Professor Gang Liu, Department of Nephrology, The Second Qilu Hospital of Shandong University, 247 Beiyuan Avenue, Jinan, Shandong 250033, P.R. China
E-mail: lg69007@163.com

Key words: renal fibrosis, histone deacetylase 3, activating transcription factor 3, Klotho, Wnt/β-catenin, NF-κB

augmented the revitalization of ECM genes associated with tissue growth factor, collagen-1α1 and plasminogen in mesangial cells. Moreover, blockade of class I histone deacetylation by the alternative HDAC suppressor MS-275 restrained TGF-β signal transduction and blocked the revitalization of kidney fibroblasts (10). HDACs are an enzyme family that removes acetyl groups from histone and non-histone proteins and they play important roles in the modulation of gene transcription and protein function (11). HDAC3 is a class I HDAC. This type of HDAC is deemed the 'classical' HDAC and the main target of current pen-HDAC inhibitors in cancer treatment (12) and in the kidney (13). Abnormal expression of HDAC3 is an essential part of CKD renal damage (14-16), indicating that HDAC3 has potential as a target for the treatment of CKD.

Activating transcription factor 3 (ATF3) belongs to the ATF/CREB transcription factor family, which is diverse in size, protein sequence and biological function, and stress-induced ATF3 can act as a transcriptional activator or inhibitor (17). ATF3 is associated with HDAC3. For example, HDAC3 mediates deacetylation of ATF3, enhancing its transcriptional inhibitory activity (18-20). There is also the possibility that ATF3 may negatively affect the binding of HDAC3 at DA-independent sites (19). In addition, ATF3 facilitates ferroptosis and renal tubular cell injury in CKD through nuclear translocation and transcriptional suppression (21-23). The transcriptional inhibition of HDAC3 is also achieved by binding to ATF3 (24). The ATF3 protein directly binds to HDAC6 and HDAC3 and does not require supernumerary proteins for binding (24). The function of ATF3 in renal fibrosis has not been extensively explored. Therefore, we hypothesize that ATF3 may influence Klotho transcription by combining with HDAC3.

The present study probed the upstream regulatory mechanism of Klotho. The results showed that Klotho produced abnormal H3K9ac modifications in renal fibrosis samples and in a TGF-β-induced HK2 cell model. This modification is mediated by HDAC3. HDAC3 combines with ATF3 to repress Klotho transcription, thereby inducing the development of renal fibrosis.

Materials and methods

Clinical samples. Renal tissues from 35 patients with CKD (kidney puncture sample) and 20 patients without CDK (paracancerous tissue of renal cancer patients) were retrieved from Yan'an Hospital of Kunming City. Among the patients with CKD who underwent renal puncture biopsy in our hospital from 2013 to 2020, the distribution of renal interstitial fibrosis in the sections obtained accounted for >75% of the total area, and the glomerular filtration rate was less than 15 ml/min/1.73 m2 calculated by EPI formula, that is, patients with stage 5 chronic kidney disease. The kidney tissue was harvested and stored at liquid nitrogen.

Cell culture. Human renal tubular HK2 cells were purchased from Otwo Biotechnology Co., Ltd. and cultured in DMEM/F12 (Gibco; Thermo Fisher Scientific, Inc.) supplemented with 10% FBS (Gibco; Thermo Fisher Scientific, Inc.) and 1% penicillin/streptomycin (MilliporeSigma) at 5% CO_2 and 37˚C. HK2 cells treated with 10 ng/ml TGF-β (cat. no. 240-B-002; R&D Systems, Inc.) for 48 h were used to construct a renal fibrosis cell model. To explore the downstream mechanisms, HK2 cells were treated with 5 μM RGFP966 (Selleck Chemicals, cat. No. S7229), a selective HDAC3 inhibitor, or an equivalent volume of vehicle (0.1% DMSO) as a control, at 37˚C for 4 h.

Cell transfection. The cells were cultured in 24-well plates overnight to reach 70-80% confluence prior to transfection. The fulllength coding sequences of Klotho and ATF3 were amplified by PCR, digested with restriction enzymes, and ligated into the pcDNA3.1(+) vector to generate the overexpression plasmids oe-Klotho and oe-ATF3. Small interfering RNA targeting ATF3 (si-ATF3), Klotho (si-Klotho), and the corresponding negative control siRNA (si-NC) were purchased from Shanghai GenePharma Co., Ltd. The siRNA sequences are listed in Table SI. For transfection, oe-Klotho (0.8 μg/well), oe-ATF3 (0.8 μg/well), si-ATF3 (50 pmol/well), si-Klotho (50 pmol/well), or si-NC (50 pmol/well) were diluted in Opti-MEM reduced serum and mixed with Lipofectamine® 3000 reagent (Invitrogen; Thermo Fisher Scientific, Inc.) according to the manufacturer's instructions. The transfection mixtures were added to at 37˚C in a humidified atmosphere containing 5% CO_2 for 6 h, after which the medium was replaced with fresh complete culture medium. The cells were cultured under the same conditions for an additional 48 h prior to subsequent experimentation. Transfection efficiency was verified by Western blot analysis.

Animals and experiments. Specific pathogen-free-grade 8-week-old male C57BL/6 mice (20±0.5 g) were obtained from the Animal Experiment Center of Kunming Medical University (Kunming, China). All animals were housed under controlled conditions at 22±2˚C with a relative humidity of 50-60%, on a 12-h light/dark cycle, and had ad libitum access to food and water. A total of 50 mice were used in the present study. The animal study was authorized by the Animal Care Committee of Yan'an Hospital Affiliated with Kunming Medical University in conformance with the institutional guidelines (approval no. 2021044). The mouse kidney fibrosis model was established using the unilateral ureteric obstruction (UUO) procedure described previously (25). In the sham-operated group, the ureter was exposed but not ligated. The mice were randomly divided into 5 groups: i) Sham-operated (Sham); ii) renal fibrosis group (UUO); iii) mice injected with si-ATF3 via the tail vein (UUO + si-ATF3, 5 nmol in 100 μl PBS, twice per week for 2 weeks) prior to UUO modeling; iv) mice were renally injected with oe-Klotho (UUO + oeKlotho, genome copy number containing $5x10^9$ virus particles) 1 week prior to UUO modeling; and v) the group in which the mice were renally injected with oeKlotho and oe-ATF3 (UUO + OE-Klotho + oe-ATF3, genome copy number containing $5x10^9$ virus particles each) 1 week prior to UUO modeling. Throughout the experiment, animal health and behaviour were monitored daily. Animals were euthanized immediately upon reaching the predefined humane endpoint: i) >15% weight loss within 1-2 days, or >20% overall weight loss; ii) signs of severe distress, including lethargy, piloerection, hunched posture, dehydration, or reduced responsiveness to external stimuli. No animals reached the humane endpoint

during the experiment. The experiment lasted for 14 days after UUO surgery. During this period, a total of 9 mice died during the experiment: 4 due to anesthesia-related complications, 3 due to surgical failure, and 2 due to postoperative infection; these animals were excluded from the final analysis. After UUO surgery for 14 days, the mice were all anesthetized by intraperitoneal injection of sodium pentobarbital (50 mg/kg body weight). Following the loss of consciousness and lack of response to toe pinch, 0.5-1 ml of whole blood was collected from each mouse via cardiac puncture for serum cytokine analysis. The blood samples were stored at room temperature for 30 min to 2 h to allow natural clotting, and serum was separated by centrifugation at 1,000 x g for 10 min at 4˚C and stored at -80˚C until further use. After blood collection, the kidneys were harvested and stored at -80˚C. All procedures were performed in accordance with institutional guidelines.

Cytokine assay. The whole blood of the mice was stored at room temperature for 30 min to 2 h. After the whole blood had naturally clotted, the serum was aspirated. The expression levels of TNF-α, IL-1β and IL-6 in mouse serum were detected using commercial ELISA kits according to the manufacturer's instructions (cat. no. PT512, PI301 and PI326; all Beyotime Biotechnology). Flow cytometric analysis was performed using a BD FACSCanto II flow cytometer (BD Biosciences).

Reverse transcription-quantitative PCR (RT-qPCR). Total RNA was extracted from tissue or cell samples via TRIzol® reagent (Invitrogen; Thermo Fisher Scientific, Inc.), and the RNA was reverse transcribed into cDNA using a First Strand cDNA synthesis kit (Beijing Genenode Biotech Co., Ltd.). SYBR Green real-time fluorescence qPCR was performed using a SYBR Green reaction mix (Beijing Solarbio Science & Technology Co., Ltd.) on a real-time PCR system (Roche LightCycler® 480 II) according to the manufacturer's protocol. The thermocycling conditions were as follows: initial denaturation at 95˚C for 2 min, followed by 40 cycles of 95˚C for 15 sec and 60˚C for 60 sec, with a final melt curve stage. GAPDH was used as the internal reference gene. The relative expression levels of target genes were calculated using the 2-ΔΔCq method (26). The primer sequences used are listed in Table I.

Table I. PCR primer sequences.

Genes	Primer	Sequence
Klotho	Forward	5'-TCCCAACCTGAGGCAACT-3'
	Reverse	5'-TGGTAGAACAAGGCTGAAGA-3'
HDAC3	Forward	5'-CGTCTTCAAGCCATACCA-3'
	Reverse	5'-GCTCCAGGATGCCAATCA-3'
GAPDH	Forward	5'-TGACCACAGTCCATGCCATCAC-3'
	Reverse	5'-CGCCTGCTTCACCACCTTCTT-3'

Western blotting. Total protein was extracted from cells or tissues with RIPA buffer (MilliporeSigma) containing 1% protease inhibitor and phosphatase inhibitor. Protein concentration was determined using a BCA protein assay kit. Equal amounts of protein (30 μg/lane) were separated by 10% SDS-PAGE and transferred to PVDF membranes. After the membranes were blocked with 5% skim milk for 2 h at room temperature, they were incubated with the primary antibody at 4˚C overnight, after which they were incubated with an HRP-conjugated secondary antibody (1:2,000; cat. no. ab205718) for 1 h at room temperature. The proteins were visualized via chemiluminescence. All western blotting experiments were repeated at least three times with independent biological samples, and representative images are shown. The protein bands were analyzed using ImageJ v1.8.0 software (National Institutes of Health). The following antibodies were used: Anti-Klotho (1:1,000; cat. no. ab181373), anti-HDAC3 (1:5,000; cat. no. ab32369; Abcam), anti-collagen I (1:1,000; cat. no. ab260043; Abcam), anti-collagen IV (1:1,000; cat. no. ab6586; all Abcam), anti-fibronectin (1:1,000; cat. no. ab2413; Abcam), anti-E-cadherin (1:1,000; cat. no. ab231303; Abcam), anti-α-SMA (1:1,000; cat. no. ab5831; Abcam), anti-ATF3 (1:1,000; cat. no. ab254268; Abcam), anti-Wnt1 (1:1,000; cat. no. ab15251; Abcam), anti-β-catenin (1:5,000; cat. no. ab32572; Abcam), anti-c-MYC (1:2,000; cat. no. ab185656; Abcam), anti-cyclin D1 (1:2,000; cat. no. ab16663; Abcam) and anti-β-actin (1:1,000; cat. no. ab8226; Abcam). The membranes were then incubated with HRP-conjugated goat anti-rabbit IgG (1:2,000; cat. no. ab205718; Abcam) or HRP-conjugated goat anti-mouse IgG (1:2,000; cat. no. ab205719; Abcam).

Histone H3 acetylation level. After the histones in each group were extracted, the acetylation level of total histone H3 was detected by a total histone H3 acetylation detection kit (cat. no. P-4030; EpigenTek Group Inc.) according to the manufacturer's instructions.

Detection of reactive oxygen species (ROS) by flow cytometry. After trypsin digestion, the concentrations of the HK2 cells in each group were adjusted using cell culture medium and 20 μl of DCFH-DA solution was added to the samples. The cells were incubated in a cell incubator in the dark for 30 min and shaken every 5 min. The cells were then centrifuged at 1,000 x g for 5 min at 4˚C and washed twice with PBS. Serum-free culture medium was added again to resuspend the cells, and the levels of ROS in the cells were measured using a flow cytometer (BD Biosciences).

Malondialdehyde (MDA) and superoxide dismutase (SOD) content assays. MDA and SOD levels in HK2 cells were measured using commercial assay kits according to the manufacturers' instructions (cat. no. BC0025; SOD kit; cat. no. BC5165; both, Beijing Solarbio Science & Technology Co., Ltd.). Briefly, the cells were lysed with RIPA lysis buffer (Beijing Solarbio Science & Technology Co., Ltd.) on ice for 30 min with vortexing every 10 min, and then centrifuged at 10,000 x g for 4 min at 4˚C. The supernatants were collected, and the MDA and SOD levels were measured according to the manufacturer's instructions.

Chromatin immunoprecipitation-qPCR (ChIP-qPCR). In brief, the cells were crosslinked with 1% polyformaldehyde at room temperature for 10 min, and the reaction was quenched with 0.125 M glycine. Then, the cells were spun down, washed, resuspended, lysed and ultrasonicated to obtain chromatin extracts. The fragmented chromatin extract was precultured with protein A/G beads (Thermo Fisher Scientific, Inc.) and incubated overnight with anti-H3K9ac antibody at 4˚C (1:50; cat. no. ab4441; Abcam). After thorough elution and reverse cross-linking, DNA was extracted for qPCR analysis.

Co-IP. The cells or tissues were harvested and lysed using IP lysis buffer (Beyotime Biotechnology; cat. no. P0013) containing protease and phosphatase inhibitors on ice for 30 min, followed by centrifugation at 12,000 x g for 15 min at 4˚C to collect the supernatants. A total of 500 μg of protein lysate was used per immunoprecipitation reaction. Protein A/G Sepharose beads (Santa Cruz Biotechnology, Inc.; cat. no. sc-2003) were pre-incubated with an anti-HDAC3 antibody (1:20; cat. no. ab32369; Abcam) at 4˚C with slow shaking for 60 min and then washed twice with lysis buffer. The antibody-bead complexes were then incubated with the lysates overnight at 4˚C with slow shaking. After immunoprecipitation, the beads were collected by centrifugation at 1,000 x g for 5 min at 4˚C and washed three times with lysis buffer. The immunoprecipitates were eluted by boiling the beads in 2x SDS-PAGE loading buffer at 95˚C for 10 min and then analyzed by Western blotting.

Masson's trichrome staining. For histological analysis, kidney tissues were fixed in 4% paraformaldehyde at room temperature for 24 h, embedded in paraffin and sectioned at a thickness of 4 μm. Masson's trichrome staining was performed to evaluate collagen deposition and renal fibrosis. Briefly, the sections were deparaffinized, rehydrated and stained using a Masson's trichrome staining kit (Beijing Solarbio Science & Technology Co., Ltd., cat. no. G1340) according to the manufacturer's instructions. The stained sections were imaged under a light microscope (Nikon Corporation). The extent of collagen deposition was assessed based on the blue-stained areas, and the images were analyzed using ImageJ v1.8.0 software (National Institutes of Health, Bethesda, MD, USA).

Immunofluorescence staining. The cells were seeded in a 24-well plate ($2x10^4$ cells/well). After 24 h, the cells were washed twice with PBS (pH 7.4), fixed with 4% paraformaldehyde for 30 min at room temperature, permeabilized with 0.5% Triton X-100 for 10 min and blocked with bovine serum albumin for 1 h at room temperature. Subsequently, the cells were incubated overnight with primary antibodies against p65 (1:100; cat. no. ab32536; Abcam) at 4˚C. The next day, the cells were incubated with Alexa Fluor 488-conjugated goat anti-rabbit IgG (1:500; cat. no. A-11008; Thermo Fisher Scientific, Inc.) for 1 h at room temperature in the dark, followed by DAPI staining (1:1,000; room temperature; 5 min). Finally, the stained cells were observed and imaged under a fluorescence microscope (Nikon Corporation).

Statistical analysis. GraphPad Prism version 8 software (Dotmatics) was used to analyze the data, and the data are presented as the mean ± standard deviation. Comparisons between two groups were performed using unpaired two-tailed Student's t-test. For comparisons involving >2 groups, one- or two-way ANOVA was used, followed by Tukey's post hoc test for multiple comparisons. $P<0.05$ was considered to indicate a statistically significant difference.

Results

Low expression of Klotho in renal fibrosis may be associated with HDAC3-mediated histone deacetylation. Studies have shown that impaired Klotho accelerates the transition of the profibrotic phenotype in renal tubular epithelial cells and strengthens the proliferation of fibroblasts, thereby promoting renal fibrosis (27-29). Accordingly, the present study used kidney tissue samples from 20 non-CKD controls and 35 patients with CKD for verification and found low expression of Klotho and high expression of HDAC3 in CKD samples (Fig. 1A and B). In addition, correlation analysis at the clinical level indicated a negative correlation between HDAC3 and Klotho (Fig. 1C). UUO is a typical model of renal fibrosis, and it has been shown that urine flow obstruction leads to extensive renal tubular lesions and fibrosis (30). After UUO-induced kidney fibrosis was established, low expression of Klotho was observed in the renal tissue of UUO mice (Fig. 2A). Western blot analysis showed decreased Klotho and increased HDAC3 in the renal tissue of UUO mice (Fig. 2B and C). Histone acetylation plays a pivotal role in the control of gene expression and is interrelated with the modulation of several diseases, including tissue fibrosis (31). This modification of histones and several non-histone proteins are under the control of histone acetyltransferase and histone deacetylases (HDACs) (32), including HDAC3. Therefore, we hypothesized that the low expression of Klotho in renal fibrosis was interrelated with HDAC3-mediated histone deacetylation. Compared with those in the sham group, histone H3 acetylation levels were reduced in the UUO group (Fig. 2D). Similarly, decreased Klotho and increased HDAC3 were observed in HK2 cells treated with TGF-β (Fig. 2E and F). Decreased histone H3 acetylation was detected in TGF-β-treated HK2 cells (Fig. 2G). These results indicate that HDAC3-mediated histone deacetylation may be observably interrelated with the abnormal downregulation of Klotho in renal fibrosis.

HDAC3 inhibits Klotho transcription and promotes HK2 cell fibrosis through histone deacetylation. K9 in histone H3 is a unique target of HDAC3, and HDAC3-mediated deacetylation of H3K9ac is important for H3K9 methylation (33), while increased H3K9ac modification acts as a transcriptional activator and can increase the levels of multiple genes. To further verify the effect of HDAC3 on renal fibrosis via the inhibition of Klotho expression through histone deacetylation, HK2 cells were treated with an HDAC3 selective inhibitor (RGFP966). ChIP-qPCR experiments showed that H3K9ac and Klotho binding was markedly decreased after TGF-β treatment while H3K9ac was increased in the Klotho group after the addition of RGFP966 (Fig. 3A), suggesting that a change in the H3K9ac level of Klotho occurs during renal fibrosis, which is associated with HDAC3. RT-qPCR and western blot analyses demonstrated that TGF-β inhibited the expression of Klotho

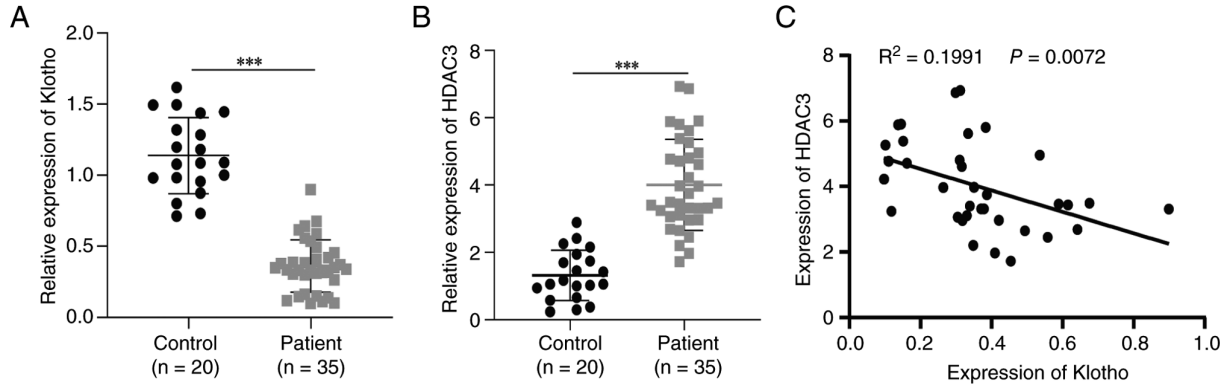

Figure 1. Expression of HDAC3 and Klotho in kidney tissues from patients with CKD and their correlation. (A) Klotho mRNA expression levels in clinical samples were assessed by RT-qPCR; (B) HDAC3 mRNA levels in clinical samples were checked by RT-qPCR; (C) Correlation analysis between Klotho and HDAC3 at the clinical level. ***P<0.001. RT-qPCR, reverse transcription-quantitative PCR.

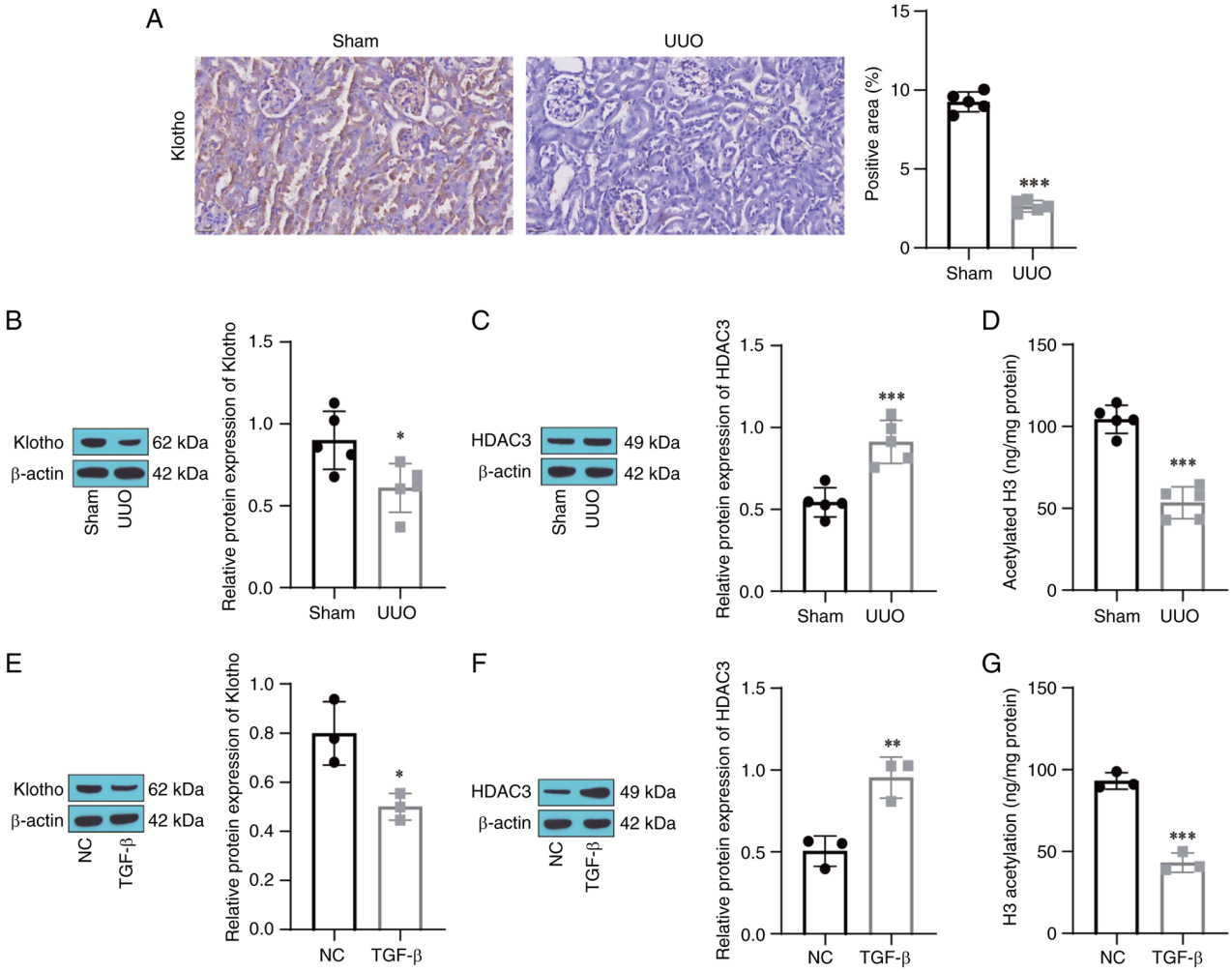

Figure 2. Low expression of Klotho in renal fibrosis may be associated with HDAC3-mediated histone deacetylation. (A) Expression levels of Klotho in renal tissues of mice were evaluated by immunohistochemical analysis. (B) Klotho and (C) HDAC3 protein levels in renal tissues of mice were detected by western blotting. (D) The levels of acetylated histone H3 in renal tissues of mice was measured using a kit. (E) Klotho and (F) HDAC3 protein expression levels in HK2 cells were detected by western blotting. (G) The expression levels of acetylated histone H3 in HK2 cells was measured using a kit. Data were analyzed using one-way ANOVA followed by Tukey's post hoc test. *P<0.05, **P<0.01, ***P<0.001 vs. the control/sham/NC group. UUO, unilateral ureteric obstruction; NC, negative control.

and that RGFP966 clearly restrained the influence of TGF-β on Klotho (Fig. 3B and C). To examine the function of HDAC3 and Klotho in renal fibrosis, two samples of si-Klotho were designed and transfected into HK2 cells. The knockdown efficiency was detected by western blotting. The results showed that compared with the si-NC group, the expression of Klotho

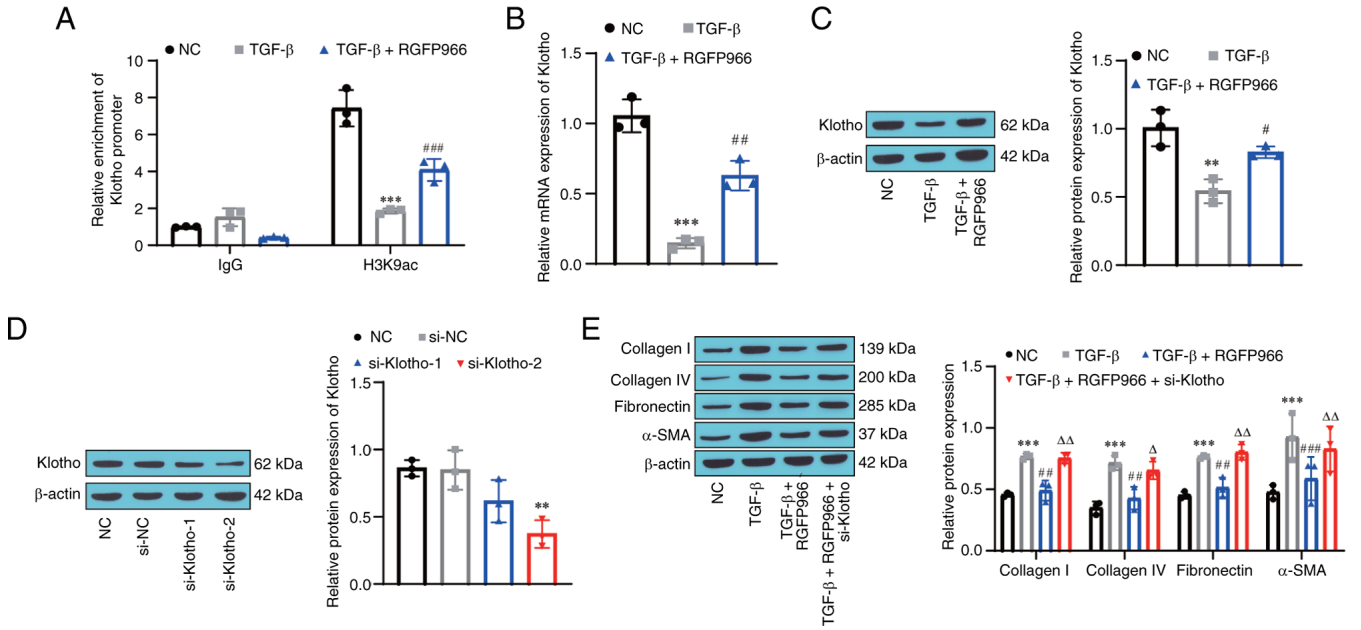

Figure 3. HDAC3 inhibits Klotho transcription and promotes HK2 cell fibrosis through histone deacetylation. (A) H3K9ac levels in the Klotho promoter region were detected by ChIP-qPCR. (B) Klotho mRNA expression levels in HK2 cells were detected by RT-qPCR. (C) Klotho protein levels in HK2 cells were detected by western blotting. (D) Validation of Klotho knockdown efficiency by siRNA in HK2 cells. (E) Collagen I, Collagen IV, Fibronectin and α-SMA protein expression levels in HK2 cells were detected by western blotting. Data were analyzed using one-way ANOVA followed by Tukey's post hoc test. **P<0.01, ***P<0.001 vs. NC group; $^{\#}$P<0.05, $^{\#\#}$P<0.01, $^{\#\#\#}$P<0.001 vs. the TGF-β group; $^{\triangle}$P<0.05, $^{\triangle\triangle}$P<0.01 vs. the TGF-β+RGFP966 group. ChIP, chromatin immunoprecipitation; RT-qPCR, reverse transcription-quantitative PCR; siRNA, small interfering RNA; α-SMA, α-smooth muscle actin; NC, negative control.

in the si-Klotho-1 and si-Klotho-2 groups decreased, where the si-Klotho-2 group showed significant differences (Fig. 3D). Subsequent experiments were conducted with si-Klotho-2. Further analysis suggested that TGF-β increased the levels of ECM-related proteins, including collagen I, Collagen IV and Fibronectin, and the fibrosis-related protein α-SMA in HK2 cells. The addition of RGFP966 prominently decreased the levels of Collagen I, Collagen IV, Fibronectin and α-SMA, and these effects were reversed by si-Klotho (Fig. 3E). These results imply suppression of HDAC3 can upregulate Klotho expression through histone acetylation, thereby suppressing TGF-β-induced fibrosis in HK2 cells.

HDAC3 binding to ATF3 transcriptionally downregulates Klotho. ATF3 can bind to HDAC3 without the need for additional proteins (24). The downregulation of Klotho was accompanied by the upregulation and nuclear translocation of ATF3, and ATF3 overexpression restrained the transcriptional activity of Klotho. Therefore, the present study speculated that HDAC3 binds to ATF3 to mediate the transcriptional repression of Klotho in renal fibrosis. Western blot analysis showed that the ATF3 protein level was markedly increased in UUO mice and in TGF-β-treated HK2 cells (Fig. 4A and B). Co-IP indicated that HDAC3 directly interacted with ATF3 both *in vitro* and *in vivo* (Fig. 4C and D). ChIP-qPCR analysis revealed that ATF3 was enriched in the Klotho promoter region after TGF-β treatment, while the binding of ATF3 to the Klotho promoter region decreased after the addition of RGFP966 (Fig. 4E). In order to explore the regulatory effect of ATF3 and HDAC3 on Klotho, the present study designed two si-ATF3 and transfected si-ATF3 into HK2 cells. Western blot analysis showed that, compared with the si-NC group, the expression of ATF3 was reduced in the si-ATF3-1 group and the si-ATF3-2 group, and the reduction of ATF3 in the si-ATF3-2 group was significantly different (Fig. 4F). si-ATF3-2 showed improved knockdown efficiency and was used for subsequent experiments. Furthermore, TGF-β inhibited the expression of Klotho in HK2 cells, and silencing ATF3 promoted the expression of Klotho (Fig. 4G and H). Consistently, to determine the ATF3-mediated effects *in vivo*, ATF3 was knocked down in mouse kidneys, as shown in Fig. S1. Similarly, lower expression of Klotho was detected in the renal tissue of UUO mice, and si-ATF3 increased the expression of Klotho (Fig. 4I). In addition, compared with those in the UOO group, si-ATF3 decreased the levels of Collagen I, Collagen IV, Fibronectin and α-SMA in the renal tissue of the mice, suggesting that ATF3 knockdown can effectively inhibit those proteins (Fig. 4J). Masson's trichrome staining showed glomerular collagen fibril hyperplasia in UUO mice, and collagen fibrils were extensively deposited in the interstitium, ATF3 knockdown decreased collagen deposition (Fig. 4K). These results point toward HDAC3 binding to ATF3 to repress Klotho transcription and promote renal fibrosis.

ATF3 mediates an inhibitory effect of Klotho on the Wnt/β-catenin signaling pathway. Blocking Wnt/β-catenin signaling may be beneficial for alleviating renal fibrosis (34-36). To explore the downstream mechanism of Klotho in kidney fibrosis, a Klotho overexpression vector was constructed (Fig. S2A) and used to treat HK2 cells and mice. Western blot analysis showed that the levels of Wnt1, β-catenin, c-MYC and Cyclin D1 were markedly increased in

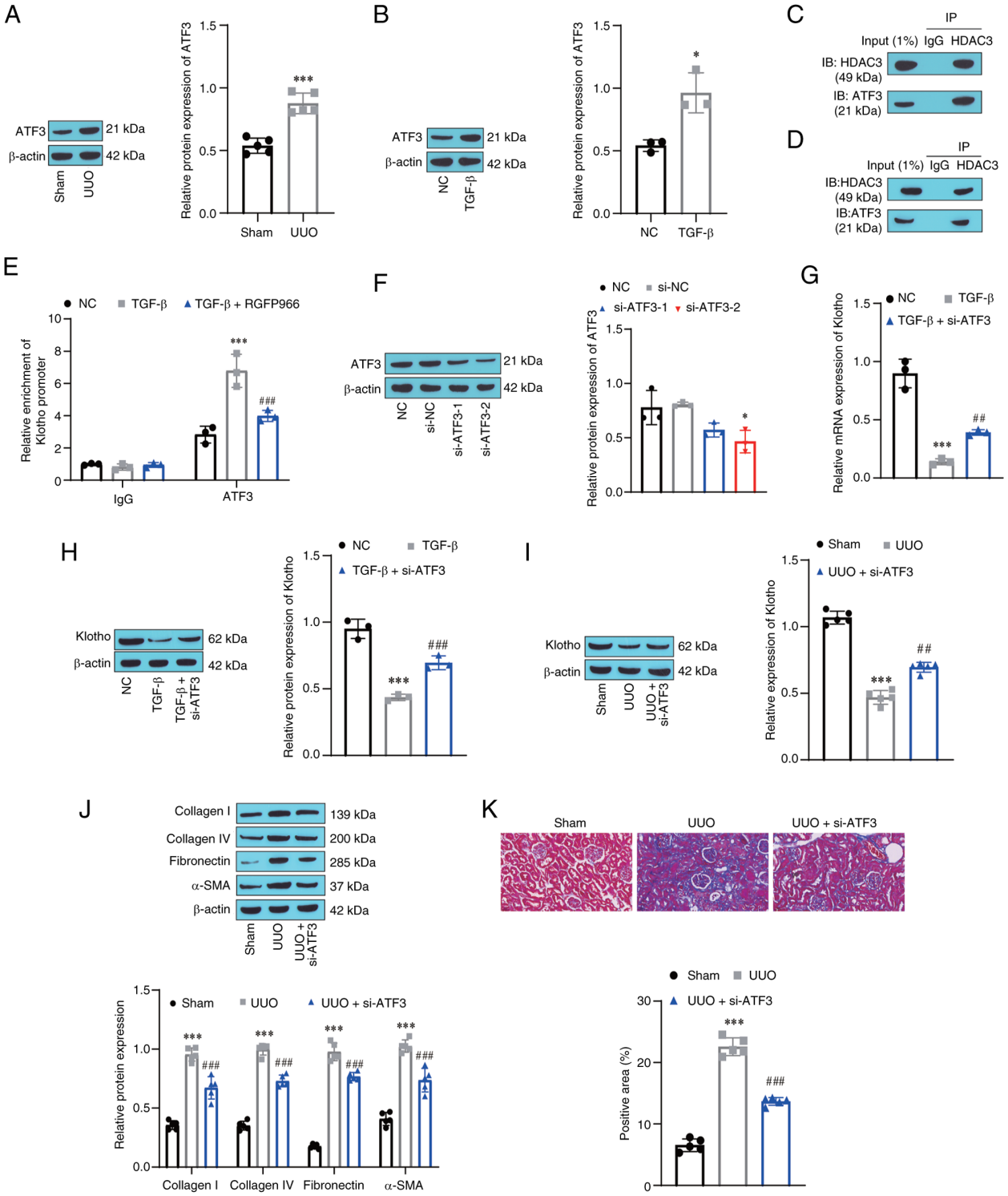

Figure 4. HDAC3 binding to ATF3 transcriptionally downregulates Klotho. (A) ATF3 protein expression in renal tissue of mice was detected by western blotting. (B) ATF3 protein expression in HK2 cells was confirmed by western blotting. The binding of (C) HDAC3 and (D) ATF3 was corroborated by coimmunoprecipitation in HK2 cells and renal tissue of mice. (E) The binding of ATF3 to the Klotho promoter region was validated by ChIP-qPCR. (F) Validation of ATF3 knockdown efficiency by siRNA in HK2 cells. (G) ATF3 mRNA expression in HK2 cells was distinguished by RT-qPCR. (H) Klotho protein expression in HK2 cells was detected by western blotting. (I) Klotho protein expression in renal tissue of mice was identified by western blotting. (J) Collagen I and IV, Fibronectin and α-SMA protein expression in renal tissue of mice were confirmed by western blotting. (K) Mouse pathological sections were observed by Masson's Trichrome staining. Data were analyzed using one-way ANOVA followed by Tukey's post hoc test. *P<0.05, ***P<0.001 vs. the NC/sham group; $^{\#\#}$P<0.01, $^{\#\#\#}$P<0.001 vs. the TGF-β group. ATF3, activates transcription factor 3; UUO, unilateral ureteric obstruction; ChIP, chromatin immunoprecipitation; RT-qPCR, reverse transcription-quantitative PCR; siRNA, small interfering RNA; α-SMA, α-smooth muscle actin; NC, negative control.

the TGF-β group, while the levels of Wnt1, β-catenin, c-MYC and Cyclin D1 were decreased in the TGF-β+oe-Klotho group; moreover, the overexpression of ATF3 prevented the aforementioned results (Fig. 5A). Compared with that in the TGF-β group, Klotho overexpression inhibited the expression of ECM-related proteins and fibrosis-related proteins, and the

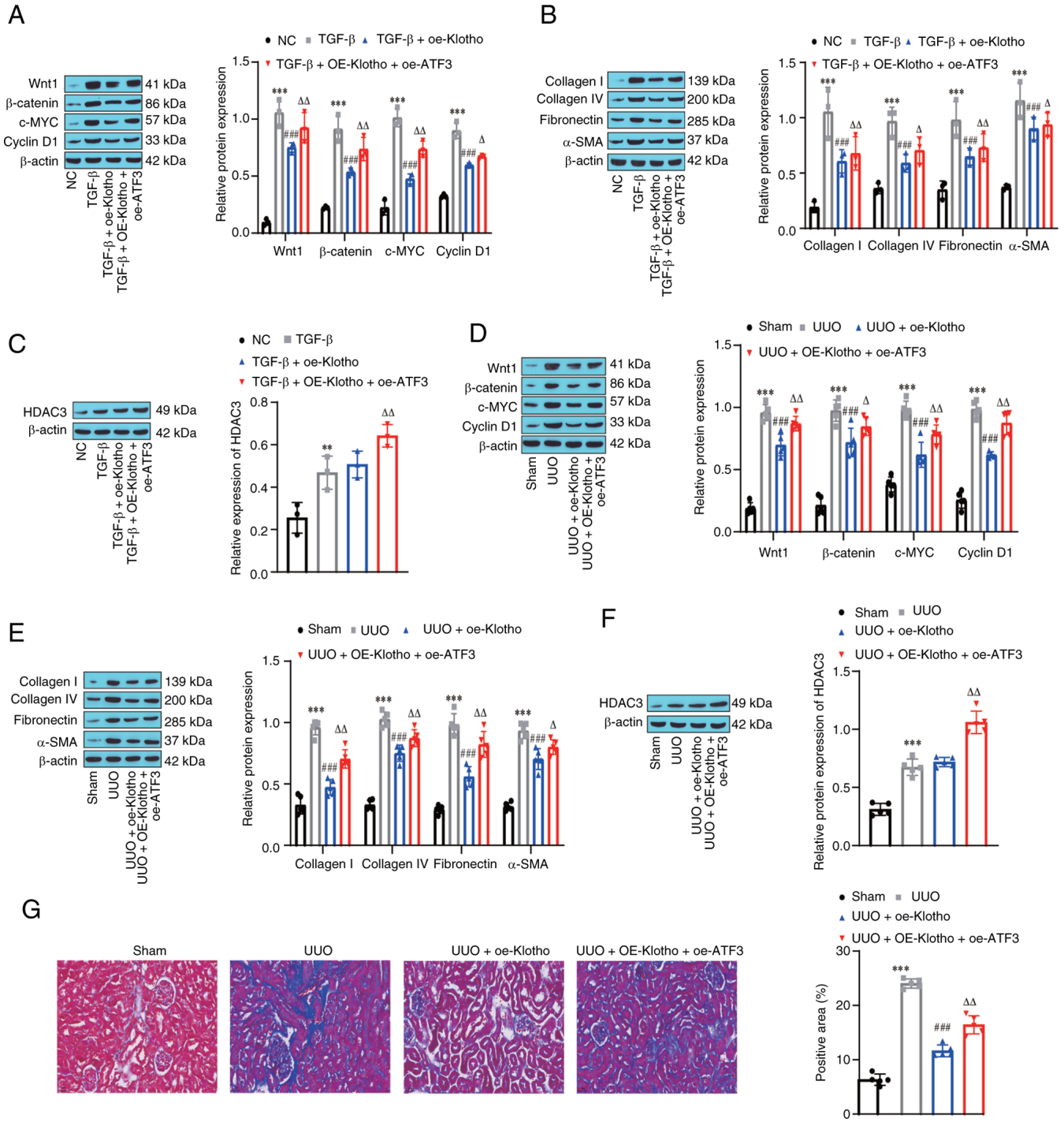

Figure 5. ATF3 mediates the inhibitory effect of Klotho on Wnt/β-catenin signaling pathway. (A) Wnt1, β-catenin, c-MYC and Cyclin D1 protein expression in HK2 cells was detected by western blotting. (B) Collagen I, Collagen IV, Fibronectin and α-SMA protein expression in HK2 cells was identified by western blotting. (C) HDAC3 protein expression in HK2 cells was detected by western blotting. (D) Wnt1, β-catenin, c-MYC and Cyclin D1 proteins in renal tissue of mice were detected by western blotting. (E) Collagen I, Collagen IV, Fibronectin and α-SMA protein expression in renal tissue of mice was detected by western blotting. (F) HDAC3 protein expression in renal tissue of mice was identified by western blotting. (G) Mouse pathological section was observed by Masson's Trichrome staining. Data were analyzed using one-way ANOVA followed by Tukey's post hoc test. **P<0.01, ***P<0.001 vs. the NC/sham group; $^{\#\#\#}$P<0.001 vs. the TGF-β/UUO group; $^{\triangle}$P<0.05, $^{\triangle\triangle}$P<0.01 vs. the TGF-β + oe-Klotho/UUO + oe-Klotho group. NC, negative control; c-MYC, cellular myelocytomatosis viral oncogene homolog; ATF3, activates transcription factor 3; UUO, unilateral ureteric obstruction; α-SMA, α-smooth muscle actin; HDAC3, histone deacetylase 3; oe, overexpression.

ATF3 overexpression vector that was constructed (Fig. S2B) increased the expression of these proteins (Fig. 5B). In addition, increased HDAC3 was detected in TGF-β-induced cells, oe-Klotho had no effect on HDAC3, while overexpression of ATF3 promoted the expression of HDAC3 (Fig. 5C). Similarly, activated Wnt/β-catenin signaling and increased renal fibrosis were observed in UUO mice. To confirm the *in vivo* effects of Klotho and ATF3, Klotho and ATF3 were overexpressed in kidney tissue (Fig. S1). Overexpression of Klotho inhibited Wnt/β-catenin signaling and the expression

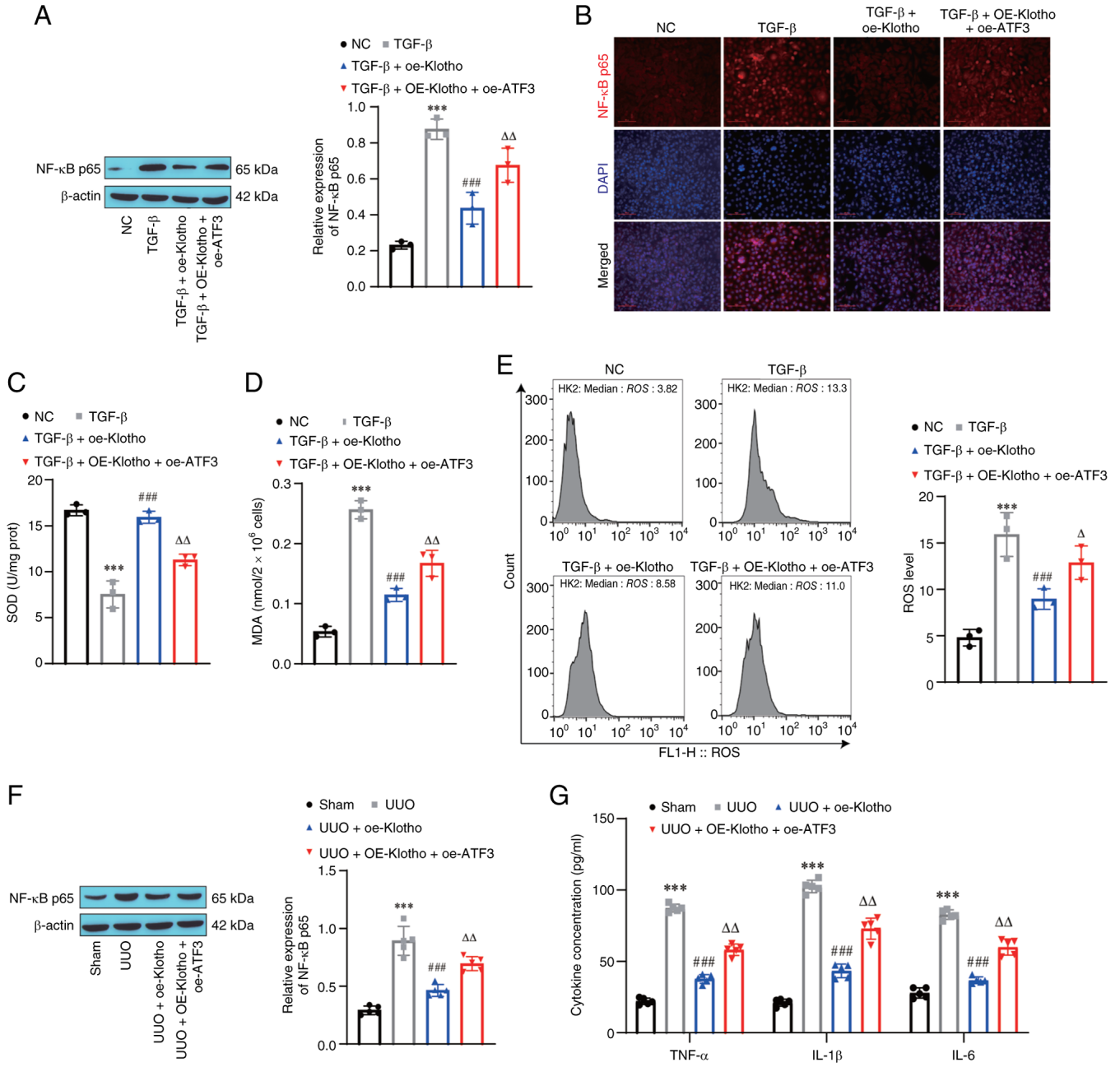

Figure 6. ATF3 mediates the inhibitory effect of Klotho on NF-κB signaling pathway. (A) NF-κB p65 protein expression in HK2 cells was detected by western blotting. (B) Nuclear translocation of NF-κB p65 in HK2 cells was observed by immunofluorescence. (C) SOD and (D) MDA levels in HK2 cells were tested by kits. (E) ROS levels in HK2 cells were tested by flow cytometry. (F) NF-κB p65 protein expression in renal tissue of mice was detected by western blotting. (G) TNF-α, IL-1β and IL-6 in mouse serum were measured by ELISA kits. Data were analyzed using one-way ANOVA followed by Tukey's post hoc test. ***P<0.001 vs. the NC/sham group; $^{\#\#\#}$P<0.001 vs. the TGF-β/UUO group; $^{\triangle}$P<0.05, $^{\triangle\triangle}$P<0.01 vs. the TGF-β + oe-Klotho/UUO + oe-Klotho group. ATF3, activates transcription factor 3; NC, negative control; UUO, unilateral ureteric obstruction; oe, overexpression.

of ECM-related proteins and fibrosis-related proteins. Further treatment of overexpression of ATF3 prevented the effect of overexpression of Klotho to some extent (Fig. 5D and E). In addition, increased HDAC3 was detected in the renal tissue of UUO mice. oe-Klotho had no effect on HDAC3, while the overexpression of ATF3 promoted the expression of HDAC3 (Fig. 5F). Masson's trichrome staining showed that glomerular collagen fibrils proliferated and were extensively deposited in the interstitium of UUO mice, and collagen deposition was significantly reduced after Klotho treatment, while overexpression of ATF3 could weaken the effect of Klotho on renal fibrosis (Fig. 5G). The results suggest that the alleviating effect of Klotho on TGF-β-induced fibrosis in HK2 cells and renal fibrosis in UUO mice may be related to the Wnt/β-catenin signaling pathway, and ATF3 prevents the inhibitory effect of Klotho on Wnt/β-catenin signaling pathway.

ATF3 mediates the inhibitory effect of Klotho on the NF-κB signaling pathway. A previous study showed that Klotho itself has antioxidant and anti-inflammatory effects and that the canonical NF-κB component RelA is one of its targets (37).

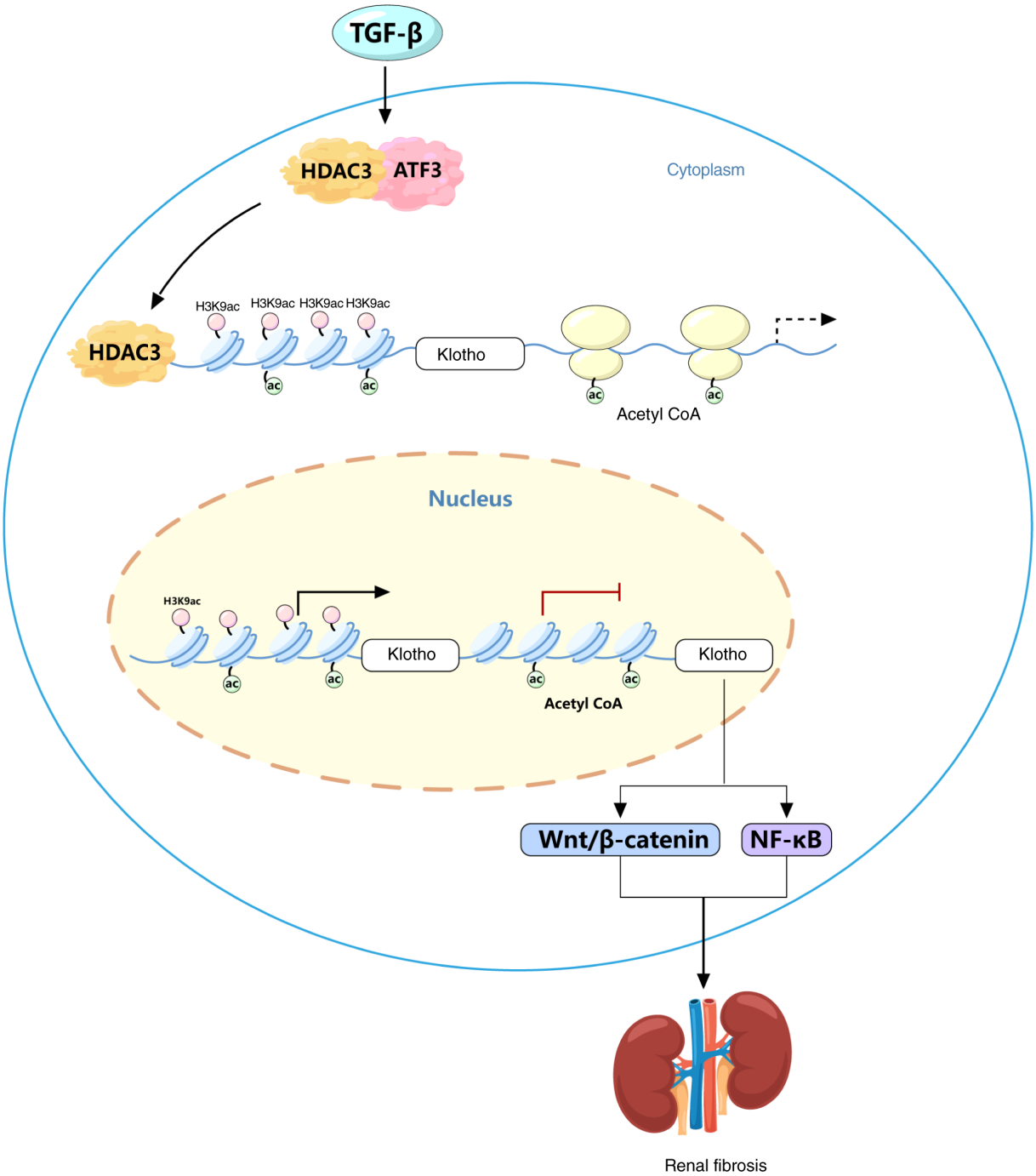

Figure 7. Mechanism diagram. Under the stimulation of TGF-β on renal tubular epithelial cells, the H3K9ac modification mediated by the binding of HDAC3 and ATF3 inhibits the transcription of Klotho. The downregulation of Klotho may further activate the Wnt/β-catenin and NF-κB pathways, thereby exacerbating renal fibrosis. HDAC3, histone deacetylase 3; ATF3, activates transcription factor 3.

Therefore, the present study subsequently detected the protein level of NF-κB. Western blot analysis indicated that the level of NF-κB p65 was increased in the TGF-β group, while NF-κB p65 was decreased after the addition of oe-Klotho, and ATF3 promoted the level of NF-κB p65 (Fig. 6A). The immunofluorescence results were consistent with the western blotting results (Fig. 6B). Moreover, TGF-β inhibited SOD levels and increased MDA and ROS levels. Compared with those in the TGF-β group, increased SOD levels and decreased MDA and ROS levels were observed after the addition of oe-Klotho. Furthermore, oe-ATF3 promoted oxidative stress and inflammation (Fig. 6C-E). Similarly, high NF-κB p65 expression was observed in the renal tissue of UUO mice, Klotho inhibited NF-κB p65 expression, and ATF3 prevented the influence of Klotho (Fig. 6F). In addition, inflammatory factor levels in murine serum were measured. UUO mice had increased levels of TNF-α, IL-1β and IL-6 and Klotho decreased the levels of these cytokines. ATF3 overexpression increased the levels of TNF-α, IL-1β and IL-6 (Fig. 6G). The results suggested that the alleviating effect of Klotho on TGF-β-induced fibrosis in HK2 cells and ATF3 prevents the inhibitory effect of Klotho on the NF-κB signaling pathway.

Discussion

Renal fibrosis is a common kidney disease characterized by depauperation and fibrosis of the renal tubules and interstitium, resulting in the gradual deterioration of renal function (38). Renal fibrosis is currently considered the typical pathological change in renal aging and CKD and is characterized by the transdifferentiation of myofibroblasts and exorbitant sedimentation of renal interstitial ECM protein (2). Currently, clinical treatments for renal fibrosis are lacking, and new methods aimed at probing the molecular biological mechanisms of renal fibrosis have shown good efficacy (39). For example, exendin-4 imparts a protective effect on renal fibrosis by binding to the GLP-1 receptor (40). Klotho, a gene involved in mammalian aging, affects various disease processes by regulating phosphate homeostasis and the activity of fibroblast growth factor family members (5). For example, the absence of Klotho can exacerbate the fibrosis process of retinal cells and induce cardiac aging and heart failure (41,42). A previous study suggests that Klotho can restrain the progression of renal fibrosis (43). Klotho defects can accelerate the transition of the profibrotic phenotype in renal tubular epithelial cells and enhance the proliferation of fibroblasts, thereby facilitating renal fibrosis (27). Use of Klotho for the treatment of renal fibrosis has been widely proposed (29,44,45). Therefore, elucidation of the upstream and downstream molecular mechanisms of Klotho could be helpful for targeting Klotho to remedy renal fibrosis.

H3K9ac modification is a major class of histone post-translational modification that represses the transcriptional activation of downstream genes by affecting nucleosomes (46). In the present study, abnormal expression of Klotho in a renal fibrosis animal model or a TGF-β-induced cell model was significantly associated with the H3K9ac modification of Klotho. Previous research also found that in renal fibrosis, Klotho has abnormal histone acetylation (47). HDACs are a family of histone deacetylases that play important roles in mediating histone modifications. To the best of our knowledge, the abnormal expression of HDAC isoforms and their role in renal fibrosis have not been consistently reported. Several class IIa HDAC inhibitors exert antifibrotic effects by reducing HDAC4 and HDAC5 levels (48). HDAC3 is a major member of the HDAC family and plays a key role in various kidney diseases (49). The clinical observation found that renal HDAC3 expression was elevated while Klotho expression was markedly reduced in patients with CKD compared with non-CKD controls, with a negative association between the two (Fig. 7). These clinical data prompted the investigation of the mechanistic link between HDAC3 and Klotho in the pathogenesis of renal fibrosis. The present study showed that HDAC3 was abnormally high in renal fibrosis and suppressed Klotho expression by inhibiting the H3K9ac modification level of Klotho and promoting the activation of fibrosis-associated proteins (Collagen-I, Collagen-IV, Fibronectin and α-SMA). Chen *et al* (50) found that selective suppression of HDAC3 and genetic knockout of HDAC3 attenuated the pathology of renal fibrosis, which was consistent with the findings of the present study and the present study further confirmed that HDAC3 repressed Klotho transcriptional activation via H3K9ac.

The function of the HDAC family is usually to act together with transcription factors with transcriptional repression activity. For example, HDAC3 binds to the transcriptional repressor ZNF22 to mediate the transcriptional repression of ZO-1, Occludin and Claudin-5, promoting blood-tumor barrier permeability in the blood-tumor barrier of tumors (51). ATF3 is one of the most widespread transcription repressors. ATF3 mediates the activation effect of LPS on inflammation by binding to HDAC3 (19,24,52). The present study showed that ATF3 was highly expressed in renal fibrosis and Sung *et al* (53) reported that high expression of ATF3 facilitates the progression of renal fibrosis. Further studies found that inhibition of HDAC3 alters the nuclear localization of ATF3 and inhibit its expression in the Klotho promoter region (18,19,24). HDAC3 inhibits H3K9ac modification in the Klotho promoter region, and conversely, ATF3 directly inhibits Klotho transcription. Klotho is commonly shown to play an important role in fibrosis-related diseases by inhibiting the activation of the Wnt/β-catenin signaling pathway to inhibit the expression of fibrotic proteins (54), and Klotho can regulate the expression of various cytokines and chemokines (55,56). In the present study, overexpression of Klotho inhibited oxidative stress and inflammation by repressing the Wnt/β-catenin and NF-κB pathways, thereby alleviating fibrosis. The overexpression of ATF3 prevented the aforementioned effects.

In brief, the present findings establish an HDAC3-ATF3-Klotho regulatory axis in which HDAC3 recruits ATF3 to the Klotho promoter, leading to Klotho transcriptional repression. Downregulation of Klotho may activate the Wnt/β-catenin and NF-κB pathways to promote oxidative stress and inflammation, thereby exacerbating the fibrotic process (Fig. 6). This result demonstrated the therapeutic potential of HDAC3-selective inhibitors for upregulating Klotho expression in the treatment of renal fibrosis disease. However, the present study did not explore other chromosomal-level modifications of Klotho, nor did it conduct relevant tests on DNA-level modifications of Klotho, which is the aim of future research. The present study only used HK2 cells to verify the phenotypes of renal fibrosis or its regulatory mechanisms. In future studies, other kidney cell lines (such as mesangial cells and renal interstitial cells) will be used to further validate the findings. One limitation of the *in vivo* experiments should be acknowledged. To confirm ATF3 knockdown in the kidney, si-ATF3 was administered in combination with other constructs (oe-Klotho and/or oe-ATF3) rather than as a single agent. While the reduced ATF3 expression observed in the UUO+si-ATF3 group compared with the UUO group supports the efficacy of si-ATF3, the present study did not include a group treated with si-ATF3 alone. Consequently, the possibility that co-administration of other constructs may have influenced ATF3 expression or the overall phenotype cannot be entirely ruled out. Future studies using si-ATF3 alone *in vivo* would be valuable to confirm the specific contribution of ATF3 knockdown in this model. Notably, HDAC inhibitors have been approved by the FDA for the treatment of skin and peripheral T-cell lymphoma and multiple myeloma (57-59). However, HDAC-based methods or drugs have not yet been used to treat kidney disease (60,61). The present study provides evidence for the application of HDAC suppressors in renal fibrosis-related diseases.

Acknowledgements

Not applicable.

Funding

This work was supported by the National Natural Science Foundation of China (grant no. 82370720) and the Science and Technology Plan Project of Yunnan Provincial Science and Technology Department (grant no. 202201AY070001-193).

Availability of data and materials

The data generated in the present study may be requested from the corresponding author.

Authors' contributions

ZY, WL and GL designed the study. ZY and XW performed the experiments. ZY, XW and HC contributed to data analysis and drafted the manuscript. ZY wrote the manuscript. ZY, XW and GL revised the manuscript. All authors read and approved the final manuscript. ZY and GL confirm the authenticity of all the raw data.

Ethics approval and consent to participate

The present study was reviewed and approved by the Animal Care Committee of Yan'an Hospital Affiliated with Kunming Medical University (Kunming, China) in conformance with the institutional guidelines (approval no. 2021044) and was carried out under the ARRIVE Guidelines 2.0.

Patient consent for publication

Not applicable.

Competing interests

The authors declare that they have no competing interests.

References

1. Mark PB, Stafford LK, Grams ME, Aalruz H, ElHafeez SA, Abdelgalil AA, Abdulkader RS, Abeywickrama HM, Abiodun OO, Abramov D, *et al*: Global, regional, and national burden of chronic kidney disease in adults, 1990-2023, and its attributable risk factors: A systematic analysis for the global burden of disease study 2023. Lancet 406: 2461-2482, 2025.
2. Zeisberg M and Neilson EG: Mechanisms of tubulointerstitial fibrosis. J Am Soc Nephrol 21: 1819-1834, 2010.
3. Woroniecki R, Gaikwad AB and Susztak K: Fetal environment, epigenetics, and pediatric renal disease. Pediatr Nephrol 26: 705-711, 2011.
4. Wing MR, Ramezani A, Gill HS, Devaney JM and Raj DS: Epigenetics of progression of chronic kidney disease: Fact or fantasy? Semin Nephrol 33: 363-374, 2013.
5. Buchanan S, Combet E, Stenvinkel P and Shiels PG: Klotho, aging, and the failing kidney. Front Endocrinol (Lausanne) 11: 560, 2020.
6. Satoh M, Nagasu H, Morita Y, Yamaguchi TP, Kanwar YS and Kashihara N: Klotho protects against mouse renal fibrosis by inhibiting Wnt signaling. Am J Physiol Renal Physiol 303: F1641-F1651, 2012.
7. Zeng Y, Wang PH, Zhang M and Du JR: Aging-related renal injury and inflammation are associated with downregulation of Klotho and induction of RIG-I/NF-κB signaling pathway in senescence-accelerated mice. Aging Clin Exp Res 28: 69-76, 2016.
8. Zhao Y, Banerjee S, Dey N, LeJeune WS, Sarkar PS, Brobey R, Rosenblatt KP, Tilton RG and Choudhary S: Klotho depletion contributes to increased inflammation in kidney of the db/db mouse model of diabetes via RelA (serine)536 phosphorylation. Diabetes 60: 1907-1916, 2011.
9. Sun G, Reddy MA, Yuan H, Lanting L, Kato M and Natarajan R: Epigenetic histone methylation modulates fibrotic gene expression. J Am Soc Nephrol 21: 2069-2080, 2010.
10. Liu N, He S, Ma L, Ponnusamy M, Tang J, Tolbert E, Bayliss G, Zhao TC, Yan H and Zhuang S: Blocking the class I histone deacetylase ameliorates renal fibrosis and inhibits renal fibroblast activation via modulating TGF-beta and EGFR signaling. PLoS One 8: e54001, 2013.
11. Singh BN, Zhang G, Hwa YL, Li J, Dowdy SC and Jiang SW: Nonhistone protein acetylation as cancer therapy targets. Expert Rev Anticancer Ther 10: 935-954, 2010.
12. Pang M and Zhuang S: Histone deacetylase: A potential therapeutic target for fibrotic disorders. J Pharmacol Exp Ther 335: 266-272, 2010.
13. Gilbert RE, Huang Q, Thai K, Advani SL, Lee K, Yuen DA, Connelly KA and Advani A: Histone deacetylase inhibition attenuates diabetes-associated kidney growth: Potential role for epigenetic modification of the epidermal growth factor receptor. Kidney Int 79: 1312-1321, 2011.
14. Lin W, Zhang Q, Liu L, Yin S, Liu Z and Cao W: Klotho restoration via acetylation of peroxisome proliferation-activated receptor γ reduces the progression of chronic kidney disease. Kidney Int 92: 669-679, 2017.
15. Wang Y, Jiao B, Hu Z and Wang Y: Critical role of histone deacetylase 3 in the regulation of kidney inflammation and fibrosis. Kidney Int 105: 775-790, 2024.
16. Chen F, Zhang L, Liu W, Zhang B, Wang S, Zhou Z, Wang W, Shen J, Deng Y and Cao W: Epigenetic suppression of RASAL1 by HDAC3 and cofactor YY1 promotes fibroblast-myofibroblast transition and renal fibrosis. Research (Wash D C) 9: 1073, 2026.
17. Cui H, Guo M, Xu D, Ding ZC, Zhou G, Ding HF, Zhang J, Tang Y and Yan C: The stress-responsive gene ATF3 regulates the histone acetyltransferase Tip60. Nat Commun 6: 6752, 2015.
18. Zhu J, Wang F, Wang L, Dai B, Xu G, Zhao L, Jiang H, Gao W, Zhang T, Zhao C, *et al*: HDAC inhibition increases CXCL12 secretion to recruit natural killer cells in peripheral T-cell lymphoma. Cancer Res 84: 2450-2467, 2024.
19. Nguyen HCB, Adlanmerini M, Hauck AK and Lazar MA: Dichotomous engagement of HDAC3 activity governs inflammatory responses. Nature 584: 286-290, 2020.
20. Li HF, Cheng CF, Liao WJ, Lin H and Yang RB: ATF3-mediated epigenetic regulation protects against acute kidney injury. J Am Soc Nephrol 21: 1003-1013, 2010.
21. Zhu B, Ni Y, Gong Y, Kang X, Guo H, Liu X, Li J and Wang L: Formononetin ameliorates ferroptosis-associated fibrosis in renal tubular epithelial cells and in mice with chronic kidney disease by suppressing the Smad3/ATF3/SLC7A11 signaling. Life Sci 315: 121331, 2023.
22. Wang L, Liu Y, Du T, Yang H, Lei L, Guo M, Ding HF, Zhang J, Wang H, Chen X and Yan C: ATF3 promotes erastin-induced ferroptosis by suppressing system Xc. Cell Death Differ 27: 662-675, 2020.
23. Tang Q, Xie J, Wang Y, Dong C and Sun Q: Exosomes secreted by ATF3/Nrf2-mediated ferroptotic renal tubular epithelial cells promote M1/M2 ratio imbalance inducing renal interstitial fibrosis following ischemia and reperfusion injury. Front Immunol 16: 1510500, 2025.
24. Darlyuk-Saadon I, Weidenfeld-Baranboim K, Yokoyama KK, Hai T and Aronheim A: The bZIP repressor proteins, c-Jun dimerization protein 2 and activating transcription factor 3, recruit multiple HDAC members to the ATF3 promoter. Biochim Biophys Acta 1819: 1142-1153, 2012.
25. Li J, Lin Q, Shao X, Li S, Zhu X, Wu J, Mou S, Gu L, Wang Q, Zhang M, *et al*: HIF1α-BNIP3-mediated mitophagy protects against renal fibrosis by decreasing ROS and inhibiting activation of the NLRP3 inflammasome. Cell Death Dis 14: 200, 2023.
26. Livak KJ and Schmittgen TD: Analysis of relative gene expression data using real-time quantitative PCR and the 2(-Delta Delta C(T)) method. Methods 25: 402-408, 2001.

27. Guan X, Nie L, He T, Yang K, Xiao T, Wang S, Huang Y, Zhang J, Wang J, Sharma K, *et al*: Klotho suppresses renal tubulo-interstitial fibrosis by controlling basic fibroblast growth factor-2 signalling. J Pathol 234: 560-572, 2014.
28. Zhang D, Li Z, Gao Y and Sun H: MiR-556-3p mediated repression of klotho under oxidative stress promotes fibrosis of renal tubular epithelial cells. Sci Rep 15: 12182, 2025.
29. Wang Y and Zhao J: The protective function of αKlotho in chronic kidney disease: Evidence and therapeutic implications. Integr Med Nephrol Androl 11: 1-11, 2024.
30. Nan QY, Piao SG, Jin JZ, Chung BH, Yang CW and Li C: Pathogenesis and management of renal fibrosis induced by unilateral ureteral obstruction. Kidney Res Clin Pract 43: 586-599, 2024.
31. Tang J and Zhuang S: Epigenetics in acute kidney injury. Curr Opin Nephrol Hypertens 24: 351-358, 2015.
32. Zhuang S: Epigenetic targeting for acute kidney injury. Nephrology (Carlton) 23 (Suppl 4): S21-S25, 2018.
33. Ji H, Zhou Y, Zhuang X, Zhu Y, Wu Z, Lu Y, Li S, Zeng Y, Lu QR, Huo Y, *et al*: HDAC3 deficiency promotes liver cancer through a defect in H3K9ac/H3K9me3 transition. Cancer Res 79: 3676-3688, 2019.
34. Xie H, Miao N, Xu D, Zhou Z, Ni J, Yin F, Wang Y, Cheng Q, Chen P, Li J, *et al*: FoxM1 promotes Wnt/β-catenin pathway activation and renal fibrosis via transcriptionally regulating multi-Wnts expressions. J Cell Mol Med 25: 1958-1971, 2021.
35. Li SS, Sun Q, Hua MR, Suo P, Chen JR, Yu XY and Zhao YY: Targeting the Wnt/β-catenin signaling pathway as a potential therapeutic strategy in renal tubulointerstitial fibrosis. Front Pharmacol 12: 719880, 2021.
36. Ma J, Jiao N, Liu X and Lu X: Saracatinib delays the progression of renal interstitial fibrosis by inhibiting the Wnt/β-catenin pathway. Kidney360 7: 25-34, 2026.
37. Izquierdo MC, Perez-Gomez MV, Sanchez-Niño MD, Sanz AB, Ruiz-Andres O, Poveda J, Moreno JA, Egido J and Ortiz A: Klotho, phosphate and inflammation/ageing in chronic kidney disease. Nephrol Dial Transplant 27 (Suppl 4): iv6-iv10, 2012.
38. Cheikh Hassan HI, Tang M, Djurdjev O, Langsford D, Sood MM and Levin A: Infection in advanced chronic kidney disease leads to increased risk of cardiovascular events, end-stage kidney disease and mortality. Kidney Int 90: 897-904, 2016.
39. Chen C, Lin XH, Xie YM, Xiong SL, Hou SZ, Huang S, Jian HL, Wen YF, Jiang XY and Liang J: Shengjiang Xiexin Decoction ameliorates DSS-induced ulcerative colitis via activating Wnt/β-Catenin signaling to enhance epithelium renovation and modulating intestinal flora. Phytomedicine 139: 156456, 2025.
40. Jia Y, Zheng Z, Guan M, Zhang Q, Li Y, Wang L and Xue Y: Exendin-4 ameliorates high glucose-induced fibrosis by inhibiting the secretion of miR-192 from injured renal tubular epithelial cells. Exp Mol Med 50: 1-13, 2018.
41. Xie L, Wang Y, Li Q, Ji X, Tu Y, Du S, Lou H, Zeng X, Zhu L, Zhang J and Zhu M: The HIF-1α/p53/miRNA-34a/Klotho axis in retinal pigment epithelial cells promotes subretinal fibrosis and exacerbates choroidal neovascularization. J Cell Mol Med 25: 1700-1711, 2021.
42. Chen K, Wang S, Sun QW, Zhang B, Ullah M and Sun Z: Klotho deficiency causes heart aging via impairing the Nrf2-GR pathway. Circ Res 128: 492-507, 2021.
43. Yuan Q, Ren Q, Li L, Tan H, Lu M, Tian Y, Huang L, Zhao B, Fu H, Hou FF, *et al*: A Klotho-derived peptide protects against kidney fibrosis by targeting TGF-β signaling. Nat Commun 13: 438, 2022.
44. Hajare AD, Dagar N and Gaikwad AB: Klotho antiaging protein: Molecular mechanisms and therapeutic potential in diseases. Mol Biomed 6: 19, 2025.
45. Nijhawan P: Soluble alpha klotho for reversal of renal interstitial fibrosis and renal regeneration: A hypothesis based on developmental biology and preclinical evidence: TH-PO0573. J Am Soc Nephrol 36 (10S): TH-PO0573, 2025.
46. Zhang Y, Zhang Q, Zhang Y and Han J: The role of histone modification in DNA replication-coupled nucleosome assembly and cancer. Int J Mol Sci 24: 4939, 2023.
47. Xia J and Cao W: Epigenetic modifications of Klotho expression in kidney diseases. J Mol Med (Berl) 99: 581-592, 2021.
48. Xiong C, Guan Y, Zhou X, Liu L, Zhuang MA, Zhang W, Zhang Y, Masucci MV, Bayliss G, Zhao TC and Zhuang S: Selective inhibition of class IIa histone deacetylases alleviates renal fibrosis. FASEB J 33: 8249-8262, 2019.
49. Zhang L and Cao W: Histone deacetylase 3 (HDAC3) as an important epigenetic regulator of kidney diseases. J Mol Med (Berl) 100: 43-51, 2022.
50. Chen F, Gao Q, Wei A, Chen X, Shi Y, Wang H and Cao W: Histone deacetylase 3 aberration inhibits Klotho transcription and promotes renal fibrosis. Cell Death Differ 28: 1001-1012, 2021.
51. Zhu B, Zhang L, Zhou X, Ning H and Ma T: Transcription factor ZNF22 regulates blood-tumor barrier permeability by interacting with HDAC3 protein. Front Mol Neurosci 15: 1027942, 2022.
52. Jeon HB and Jang Y: Reversible inactivation of bovine plasma amine oxidase by cysteamine and related analogs. Biochem Biophys Res Commun 403: 442-446, 2010.
53. Sung CC, Poll BG, Lin SH, Murillo-de-Ozores AR, Chou CL, Chen L, Yang CR, Chen MH, Hsu YJ and Knepper MA: Early molecular events mediating loss of aquaporin-2 during ureteral obstruction in rats. J Am Soc Nephrol 33: 2040-2058, 2022.
54. Miao J, Liu J, Niu J, Zhang Y, Shen W, Luo C, Liu Y, Li C, Li H, Yang P, *et al*: Wnt/β-catenin/RAS signaling mediates age-related renal fibrosis and is associated with mitochondrial dysfunction. Aging Cell 18: e13004, 2019.
55. Guo Y, Zhuang X, Huang Z, Zou J, Yang D, Hu X, Du Z, Wang L and Liao X: Klotho protects the heart from hyperglycemia-induced injury by inactivating ROS and NF-κB-mediated inflammation both in vitro and in vivo. Biochim Biophys Acta Mol Basis Dis 1864: 238-251, 2018.
56. Lai L, Li Y, Liu J, Luo L, Tang J, Xue J and Liu T: Bovine serum albumin aggravates macrophage M1 activation and kidney injury in heterozygous Klotho-deficient mice via the gut microbiota-immune axis. Int J Biol Sci 17: 742-755, 2021.
57. Chun P: Histone deacetylase inhibitors in medical therapeutics. In: Medical Epigenetics. Elsevier, pp633-655, 2016.
58. Li Y, Wang F, Chen X, Wang J, Zhao Y, Li Y and He B: Zinc-dependent deacetylase (HDAC) inhibitors with different zinc binding groups. Curr Top Med Chem 19: 223-241, 2019.
59. El Omari N, Bakrim S, Elhrech H, Aanniz T, Balahbib A, Lee LH, Al Abdulmonem W and Bouyahya A: Clinical efficacy and mechanistic insights of FDA-approved HDAC inhibitors in the treatment of lymphoma. Eur J Pharm Sci 208: 107057, 2025.
60. Cappellacci L, Perinelli DR, Maggi F, Grifantini M and Petrelli R: Recent progress in histone deacetylase inhibitors as anticancer agents. Curr Med Chem 27: 2449-2493, 2020.
61. Li J, Yu C, Shen F, Cui B, Liu N and Zhuang S: Class IIa histone deacetylase inhibition ameliorates acute kidney injury by suppressing renal tubular cell apoptosis and enhancing autophagy and proliferation. Front Pharmacol 13: 946192, 2022.